IOPscience iopscience.iop.org

Home Search Collections Journals About Contact us My IOPscience

One-step sculpting of silicon microstructures from pillars to needles for water and oil repelling surfaces

This article has been downloaded from IOPscience. Please scroll down to see the full text article.

2013 J. Micromech. Microeng. 23 025004

(http://iopscience.iop.org/0960-1317/23/2/025004)

View the table of contents for this issue, or go to the journal homepage for more

Download details:
IP Address: 130.89.112.126
The article was downloaded on 16/01/2013 at 15:19

Please note that terms and conditions apply.

J. Micromech. Microeng. **23** (2013) 025004 (6pp) doi:10.1088/0960-1317/23/2/025004

One-step sculpting of silicon microstructures from pillars to needles for water and oil repelling surfaces

A Susarrey-Arce, Á G Marín, S Schlautmann, L Lefferts, J G E Gardeniers and A van Houselt[1]

Catalytic Processes and Materials, Mesoscale Chemical Systems and Physics of Fluids, MESA+ Institute for Nanotechnology, Faculty of Science and Technology, University of Twente, PO Box 217, 7500 AE Enschede, The Netherlands

E-mail: A.vanHouselt@utwente.nl

Received 8 October 2012, in final form 16 November 2012
Published 21 December 2012
Online at stacks.iop.org/JMM/23/025004

Abstract

Surfaces that repel both water and oil effectively (contact angles > 150°) are rare. Here we detail the microfabrication method of silicon surfaces with such properties. The method is based on careful tuning of the process conditions in a reactive etching protocol. We investigate the influence of SF_6, O_2 and CHF_3 gases during the etching process using the same pitch of a photolithographic mask. Varying the loading conditions during etching, we optimized the conditions to fabricate homogeneous pedestal-like structures. The roughness of the microstructures could also effectively be controlled by tuning the dry plasma etching conditions. The wetting behavior of the resulting microstructures was evaluated in terms of the water and oil contact angles. Excitingly, the surfaces can be engineered from superhydrophobic to omniphobic by variation of the aforementioned predefined parameters.

(Some figures may appear in colour only in the online journal)

Introduction

Superhydrophobicity [1] and superoleophobicity [2] have attracted particular attention over the last decade, during which new methodologies have become available to establish water, oil or organic solvent repellency [3–6]. Besides the choice of a specific roughness and chemical composition, a good control of the shape of the micro and/or nanofeatures on the surface is critical to achieve these special properties. A surface is superhydrophobic (superoleophobic) when the contact angle (CA) between the water (oil) droplets and the surface is above 150° [6]. Nature-inspired superhydrophobic (superoleophobic) materials with lotus leaf-like micro and nano bumps [7] and waterstrider leg mimicking features [8] have been reported. These artificial surfaces are fabricated via different methods [9], including plasma etching [10], soft imprinting lithography [11], backside 3D diffuser lithography [12], physical or chemical vapor deposition [13] and electrochemical synthesis [14].

Reports on combined superhydrophobic and superoleophobic properties in one surface structure in order to establish so-called 'omniphobicity' are, however, much scarcer [15–19]. An appealing recent example can be found in the work of Im *et al* who report the fabrication of inverse trapezoidal polydimethylsiloxane (PDMS) microstructures [20].

Recently we have reported two studies on the evaporation of droplets on omniphobic surfaces which consisted of an array of micromachined pillars with a variety of special shapes, including overhanging structures [21–22]. In the present communication we will detail the fabrication process and determine the key fabrication parameters to obtain an omniphobic surface.

Experimental method

Arrays of microstructures were fabricated by reactive ion etching (RIE) of a silicon wafer (*p*-type, Boron doped

[1] Author to whom any correspondence should be addressed.

 © 2013 IOP Publishing Ltd Printed in the UK & the USA

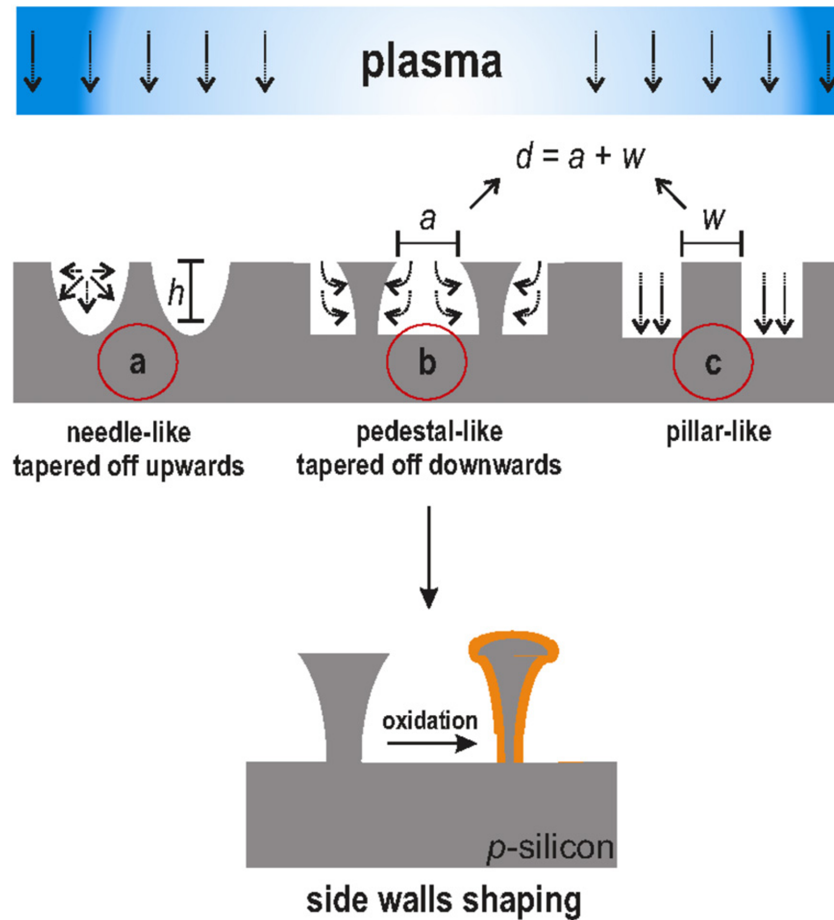

Figure 1. Schematic of the microstructure fabrication. Reactive ion etching is used to tune the microstructure shapes to (a) needle-like with smothered or sharp edges, (b) negative tapered (pedestal-like) structure and (c) straight pillar structure; where, *h* is defined as the microstructure height, *a* microstructure interspace and *w* microstructure top diameter. An oxidation step to shape the pedestal-like structure is illustrated and indicated by an arrow in (*b*).

5–10 Ohm cm resistivity, 100 mm diameter, 525 μm thickness, {100} crystal orientation; Okmetic Finland) which was covered by a patterned photoresist layer. The OiR 907/17 photoresist was spun on the silicon wafer at 4000 rpm for 30 s to obtain a layer thickness of 1.7 μm. After a soft-bake step at 95° C for 90 s, the photoresist layer was exposed for 3.5 s to mid-UV light in an EVG 620 mask aligner through a photomask which contained the microstructure array geometry. Subsequently the wafers were immersed for 1 min in OPD-4262 and the patterned resist layer was hard-baked at 120 °C for 30 min in air.

The RIE was carried out on two different machines: (1) on an Electrotech Plasmafab 310–340 parallel-plate twin deposition/etch system, and (2) on an Adixen AMS100 SE ICP system. We will refer to these systems as RIE-1 and RIE-2, respectively. The etching time for experiments on RIE-1 was kept constant at 10 min, and on RIE-2 at 5 min. The chamber pressure in both systems was set to 75 mTorr. The electrode with the attached silicon substrate was kept at 10 °C for RIE-1 and at –50 °C for RIE-2, using liquid nitrogen as coolant in the latter system. The gas flows of SF_6 and O_2 during the etching process were used as tuning-variables on both systems, as well as the presence or absence of a plasma shower head (PSH) on RIE-1. The RF plasma power on system RIE-1 and the ICP plasma power on RIE-2 were varied, while on RIE-2 a constant CCP power of 20 W and a source power of 500 W were maintained. A constant CHF_3 flow of 10 sccm was applied in RIE-1. After both RIE-steps, the photoresist was removed from the wafers by oxygen plasma cleaning, HNO_3 cleaning and a 1% HF dip.

In addition, to achieve smoothening of the sides of the microstructure, 1 μm of SiO_2 was grown by steam oxidation (1150 °C). Because oxidized silicon occupies an approximately 40% larger volume than unoxidized silicon, this procedure leads to the rounding off of the sharp edges of the structures, as illustrated in figure 1. The oxide thickness was controlled carefully to avoid a collapse of the microstructures due to 'over-oxidation'.

Schematic representations of the three distinct microstructures, achieved by the varied etch parameters, are sketched in figure 1 (*a*): needle-shaped (tapered off upward) microstructures (*a*); pedestal-shaped (tapered off downward) microstructures (*b*) and pillar-shaped microstructures (*c*).

Finally, the silicon microstructures were coated by vapor deposition in a vacuum system using trichloro (1H, 1H, 2H, 2H-perfluorooctyl) silane (FOTS 97%, Sigma-Aldrich). CA measurements were carried out at room temperature (21 °C), with a relative humidity of 35% using Dutch water (Millipore

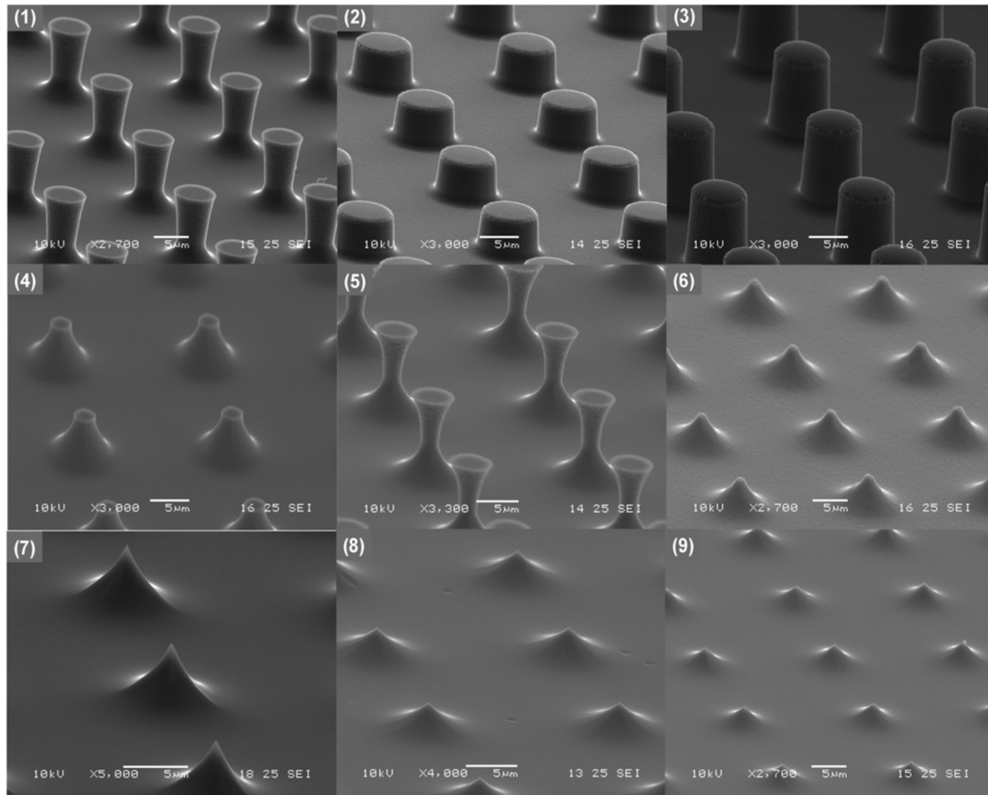

Figure 2. Microstructure patterns made with system RIE-1. In each SEM image the scale bar represents 5 μm. Each inset number is related to the parameters listed in table 1.

Table 1. RIE-1 experimental parameters employed to fabricate shaped microstructures.

	Sample								
Parameters	1	2	3	4	5	6	7	8	9
Plasma shower (PSH)	yes	yes	yes	no	no	no	yes	no	yes
O_2 [sccm]	5	20	20	5	5	5	20	20	5
RF power [W]	75	75	150	75	75	150	150	150	150
SF_6 [sccm]	30	30	30	30	50	50	50	50	50

Milli-Q system, resistivity 18.2 MΩ cm), commercial olive oil and *n*-octane (99%, Alfa Aesar).

Results

Microstructure shapes obtained with system RIE-1

In order to achieve a good control of the etched silicon microstructures, we varied the gas concentrations of SF_6, O_2 and CHF_3, since these concentrations influence the shape of the microstructures via a synergetic ion-inhibition mechanism. The surface passivation [23] is balanced with the ionic surface bombardment, via the parameters O_2 and SF_6 flow and plasma power [24, 25]. In addition, the presence of CHF_3 leads to semi-isotropic etching profiles [26]. The systematic variations in the SF_6, O_2 and CHF_3 concentrations and the presence of a PSH during the etching process for 9 different etching procedures are shown in table 1. In figure 2 the resulting microstructures are shown.

In figure 2(1)–(3), pillar-like microstructures can be observed. The pillars in figure 2(1) are slightly tapered off downward, while in figures 2(2) and (3) the pillars are straight. The difference between figures 2(1) and (2) is the amount of O_2 addition to SF_6/CHF_3 plasma (11 vol% and 33 vol% from the total plasma gas mixture). In addition, the height of the pillars reduces by $\sim$3 μm going from figures 2(1) to (2), possibly due to a lower surface coverage with fluorine atoms which changes the surface chemistry from primarily Si–C to Si–F, and next to Si–O bonding, as the O_2 concentration is increased further (since the SF_6 and CHF_3 contributions to the plasma are changed from 66 vol% and 22 vol% in figure 2(1) to 50 vol% and 16 vol%, respectively, in figure 2(2)). It has also been suggested that a passivation layer of SiO_xF_y leads to a decrease in the etching rate perpendicular to the substrate surface [26]. To develop higher cylindrical microstructures, the conditions are maintained as in figure 2(2), but the RF plasma power is increased from 75 to 150 W in figure 2(3). With these conditions, higher and straight pillars are obtained with a height of about 8.55 μm. The increased RF plasma power also leads to an increase in the silicon etching rate from 0.40 μm min^{-1} (in figure 2(2)) to 0.85 μm min.$^{-1}$ (in figure 2(3)). Without a PSH (figure 2(4)), the etching is more isotropic (then with a PSH, figure 2(1)), resulting in microstructures which are tapered off upward with a top diameter of $\sim$ 1.2 μm, against 2.3 μm in the case of figure 2(1)).

An increase in the SF_6 flow to 50 sccm, while the other parameters in figure 2(4) are kept constant, leads to pillars with well-defined smooth concave sides (figure 2(5)). These

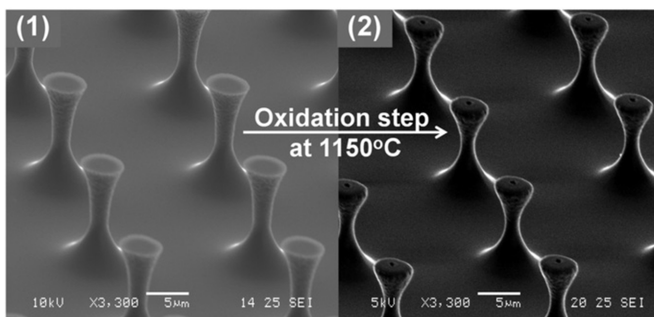

Figure 3. SEM image of the pedestal-like structures, before and after the thermal oxidation process.

'pillars' have an overhanging top plateau. The angle between their sides and the top surface (measured in the dense phase) is ~60°.

In figures 2(5)–(9), the combination of the increased SF_6 flow and the other preparation parameters (presence of a PSH, O_2 and CHF_3 flow and RF power) leads to faster (compared to figure 2(4)) and isotropic etching, which results in sharp tips. The increased vertical and lateral etching rates originate possibly from a thinner passivation layer, due to a higher surface coverage with fluorine atoms, which leads to a primarily Si–C surface chemistry, as discussed above. The maximum height difference between the sharp needles (between figures 2(7) and (9)) is ~0.7 μm.

The result of a subsequent steam oxidation step of the microstructures shown in figure 2(5), is shown in figure 3. The interfaces of these pedestal-like microstructures are more smooth after the oxidation step.

Compared to reported omniphobic [27, 28], or superhydrophobic [29] similarly micropatterned [30, 10] Si surfaces, our procedure results in a very precise control of the surface structure and interface smoothness, which enables one to verify systematically the influence of both surface roughness and edge-curvature on the wetting properties of these surfaces [22].

Microstructure shapes obtained with system RIE-2

Microstructures grown in the RIE-2 system were fabricated using a SF_6 flow of 100 sccm, a CCP power of 20 W and a source power of 500 W, without a PSH. The effect of the addition of O_2 to the plasma was systematically investigated (see figure 4(1)–(5)). Due to the high SF_6 concentration, the microstructures in figure 4(1) are mainly needle-like. An increase in the O_2 flow in figure 4(2)–(5) results in more anisotropic etching, in combination with a lower etching rate. In figure 4(2) the sides of the pillars are composed of porous nanoflakes. In figure 4(4) some small needles are present on the surface in between the micropillars, suggesting the presence of 'black silicon' at higher O_2 concentrations. In fact, in figure 4(5), a field of nanograss 'black silicon' [25] is obtained at 50 sccm O_2 flow. Figure 4(6), shows square microtables with rough, porous sidewalls. The square nature arises from crystal-orientation-dependent etching, due to the relatively low influence of ion bombardment under these conditions, an effect that has been reported before for similar conditions [24].

Wetting behavior of the fabricated structures

For the case when a liquid wets only the top of the microstructures on the surface, leaving air underneath the

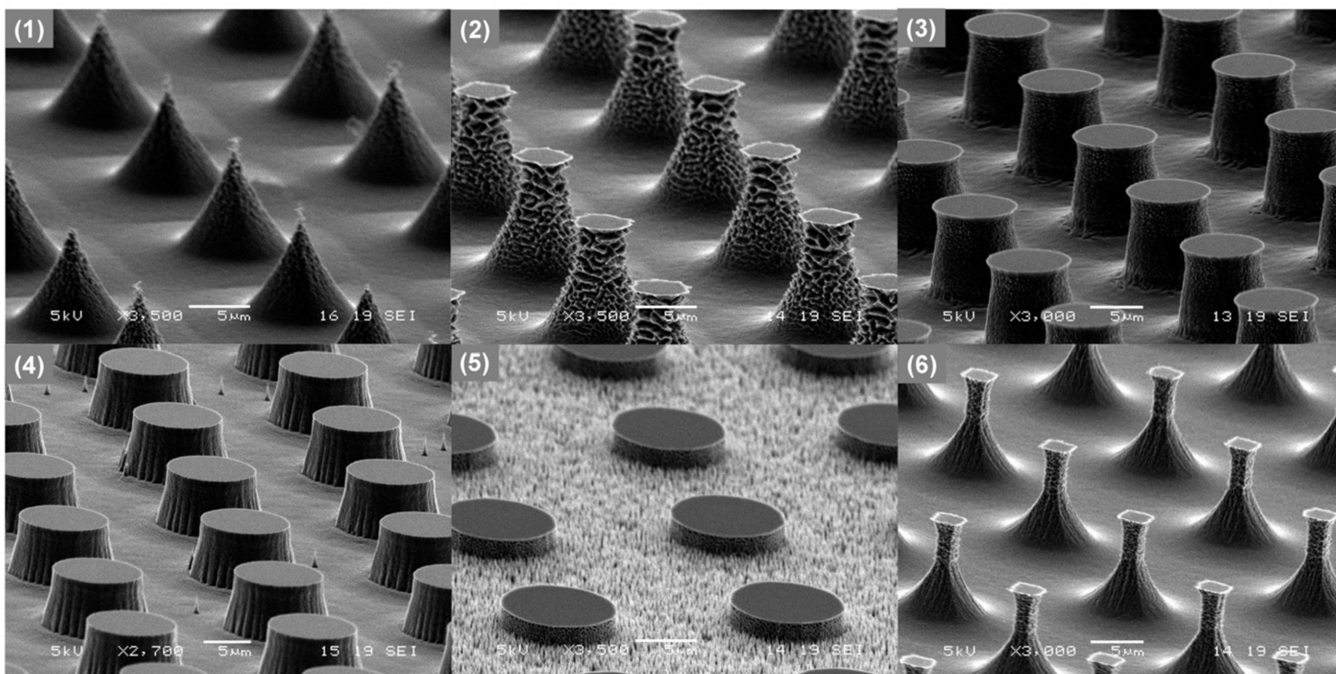

Figure 4. Microstructure patterns made with system RIE-2. In each SEM image the scale bar represents 5 μm. The O_2 flow used in the etching process was as follows: (1) 17.5 sccm, (2) 20 sccm, (3) 25 sccm, (4) 35 sccm and (5) 50 sccm for 5 min. Sample (6) was processed in two steps: 25 sccm for 2.5 min, followed by 15 sccm for 2.5 min.

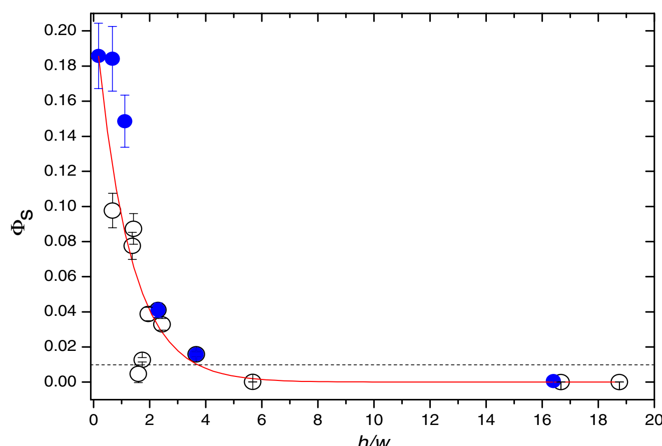

Figure 5. Pillar density Φ_s as a function of h/w. Microstructures fabricated by RIE-1 are shown as open circles and microstructures fabricated by RIE-2 are shown as closed circles.

droplet between the microstructures, Cassie and Baxter came up with an equation for the apparent CA θ^* in terms of the CA θ on the chemically equivalent flat surface: $\cos\theta^* = -1 + \Phi_s (1 + \cos\theta)$, where Φ_s is the fraction of the top-surface area of the microstructures from the total surface area [31] or, in other words, the top-area packing fraction. In figure 5, we show the top-area packing fraction Φ_s, calculated as $(\pi/4)(\mathrm{w}/\mathrm{d})^2$, as function of h/w (with h, w and d as defined in figure 1). The points in figure 5 essentially follow a hyperbola (indicated by the solid line), since Φ_s, which is proportional w^2, is plotted against h/w. The points above the dotted line ($\Phi_s > 0.01$) in figure 5 are accompanied by superhydrophobic behavior, as evidenced in figure 6(1)–(5). The points below the dotted line ($\Phi_s < 0.01$) are accompanied by lower contact angles (see for instance figure 6(6)), most probably because the droplets are not in the CassieBaxter state on these sharp needles. These observations are in agreement with other studies with observed droplets in the CassieBaxter state for values of Φ_s around 0.02 [31] to 0.20 [33]. In addition, it is important to note that is possible to change the top-area packing fraction Φ_s, even when the pitches of the masks are identical, to the so-called loading effects in RIE [24].

Furthermore, in addition to superhydrophobicity, some of the fabricated microstructures also exhibit superoleophobicity, repelling both water and oil very effectively, as evidenced by the photographs of drops of water, olive-oil and n-octane on the substrate in figure 7. This so-called 'omniphobicity' could be related to the re-entrant surface curvature or, in other words, the 'over-hanging' microstructures [20]. The substrates, which show omniphobicity, also show a remarkable stability against the wetting transition during water evaporation [22]. In comparison with most other fabrication methods for omniphobic surfaces, which were recently reported by Wilke *et al*, Wu *et al* and Tuteja *et al* [16, 27, 28, 34], the control of the surface roughness of the micropillars, which is shown

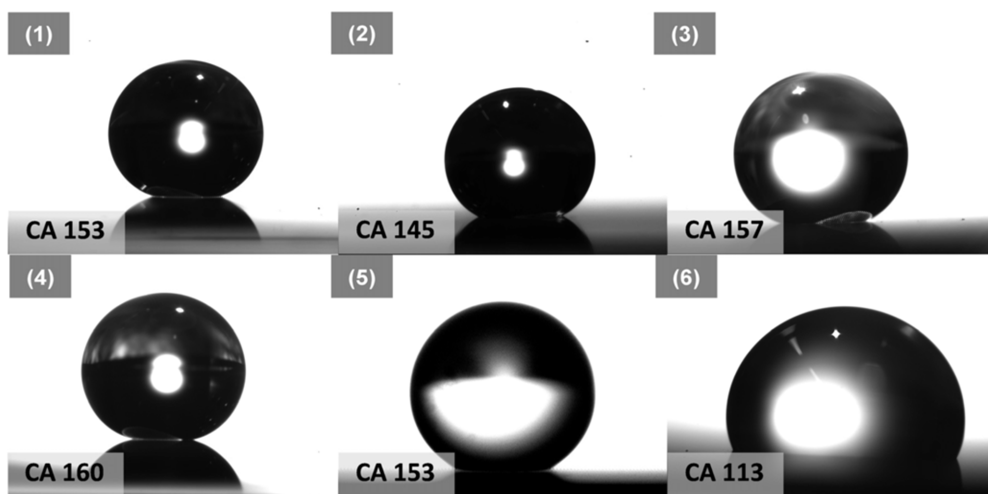

Figure 6. Side photographs of water droplets on the surfaces fabricated by RIE-1. The numbers correspond to the numbers in figure 2. The contact angle value is shown in the inset.

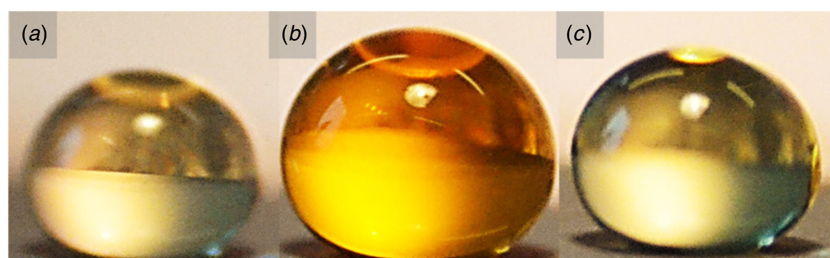

Figure 7. Side-photographs of droplets of (*a*) n-octane (left, $\sigma_t = 21.6$ mN m^{-1}), (*b*) water (middle, $\sigma_t = 72.8$ mN m^{-1}) and (*c*) olive oil (right, $\sigma_t = 32.5$ mN m^{-1}) on a negatively tapered substrate made by RIE-2, similar to figure 4(2). In all cases the contact angle is ~160°.

to have an influence on the wetting properties [22], is well controlled in our method. Recently, also Zhao *et al* reported the microfabrication of oil-repellent surfaces [19] with a well-controlled side roughness.

In short, by controlling effectively the top width of the prepared microstructures, we were able to produce superhydrophobic, and in some cases even omniphobic, surfaces. The shape and roughness of the surfaces of the produced microstructures, which are of key-importance for the wetting behavior, can be controlled by the appropriate choices of the dry-etching parameters. The influence of these parameters can possibly be explained in terms of the etching rate. In RIE-1 the etching rate is lower, due to the presence of CHF_3 in the plasma, [35] resulting in smoother surfaces compared to RIE-2.

Conclusions

Two silicon dry-etching methods to create various microstructures by varying the gas loading during RIE using a single mask-layer etching procedure have been described. The edges and shapes were well-controlled by varying the O_2/SF_6 gas loading, the plasma power and the presence of a plasma shower head. This method allows the growth of many different shapes, like pillars, needles, tipis and pedestals, with one mask. In both cases, the more pillar-like microstructured surfaces exhibit hydrophobic, and in some case even omniphobic, behavior.

Acknowledgment

The authors gratefully acknowledge to Dr Roald M Tiggelaar for his valuable scientific comments. This work is financially supported by NWO under grant no 700.58.041 and no700.10.408

References

[1] Quéré D 2008 *Annu. Rev. Mater. Res.* **38** 71–99
[2] Hsieh C-T, Wu F-L and Chen W-Y 2010 *Mater. Chem. Phys.* **121** 14–21
[3] Liu M, Liu X, Ding C, Wei Z, Zhu Y and Jiang L 2011 *Soft Matter* **7** 4163–5
[4] Yao X, Gao J, Song Y and Jiang L 2011 *Adv. Funct. Mater.* **21** 4270–6
[5] Im M, Im H, Lee J-H, Yoon J-B and Choi Y-K 2006 *Langmuir* **26** 17389–97
[6] Li X-M, Reinhoudt D and Crego-Calama M 2007 *Chem. Soc. Rev.* **36** 1350–68
[7] Bhushan B and Jung Y C 2006 *Nanotechnology* **17** 2758–72
[8] Zhang X, Zhao J, Zhu Q, Chen N, Zhang M and Pan Q 2011 *ACS Appl. Mater. Interfaces* **3** 2630–6
[9] Fürstner R and Barthlott W 2005 *Langmuir* **21** 956–61
[10] Azimi S, Sandoughsaz A, Amirsolaimani B, Naghsh-Nilchi J and Mohajerzadeh S 2011 *J. Micromech. Microeng.* **21** 074005
[11] Wu D, Wu S-Z, Chen Q-D, Zhang Y-L, Yao J, Yao X, Niu L-G, Wang J-N, Jiang L and Sun H-B 2011 *Adv. Mater.* **23** 545–9
[12] Lee J-H, Choi W-S, Lee K-H and Yoon J-B 2008 *J. Micromech. Microeng.* **18** 125015
[13] Zhang X, Shi F, Niu J, Jiang Y and Wang Z 2008 *J. Mater. Chem.* **18** 621–33
[14] Zhao N, Shi F, Wang Z and Zhang X 2005 *Langmuir* **21** 4713–6
[15] Meng H, Wang S, Xi J, Tang Z and Jiang L 2008 *J. Phys. Chem. C* **112** 11454–8
[16] Tuteja A, Choi W, Ma M, Mabry J M, Mazzella S A, Rutledge G C, McKinley G H and Cohen R E 2007 *Science* **318** 1618–22
[17] Wu W, Wang X, Wang D, Chen M, Zhou F, Liu W and Xue Q 2009 *Chem. Commun.* **1043** 1043–5
[18] Cao L, Price T P, Weiss M and Gao D 2008 *Langmuir* **24** 1640–3
[19] Zhao H, Law K-Y and Sambhy V 2011 *Langmuir* **27** 5927–35
[20] Im M, Im H, Lee J-H, Yoo J-B and Choi Y-K 2010 *Soft Matter* **6** 1401–4
[21] Marín A G, Gelderblom H, Susarrey-Arce A, van Houselt A, Lefferts L, Gardeniers H, Lohse D and Snoeijer J H 2012 Building micro-soccer-balls with evaporating colloidal fakir drops *Proc. Natl Acad. Sci.* **109** 16455–8
[22] Susarrey-Arce A, Marín A G, Nair H, Lefferts L, Gardeniers J G E, Lohse D and van Houselt A 2012 *Soft Matter* **8** 9765
[23] Oehrlein G S, Robey S W and Lindström J L 1988 *Appl. Phys. Lett.* **52** 1170–2
[24] de Boer M J, Gardeniers J G E, Jansen H V, Smulders E, Gilde M-J, Roelofs G, Sasserath J N and Elwenspoek M 2002 *J. Microelectromech. Syst.* **11** 385–401
[25] Jansen H, de Boer M, Legtenberg R and Elwenspoek M 1995 *J. Micromech. Microeng.* **5** 115–20
[26] Legtenberg R, Jansen H, de Boer M and Elwenspoek M 1995 *J. Electrochem. Soc.* **6** 2020–7
[27] Tuteja A, Choi W, Mabry J M, McKinley G H and Cohen R E 2008 *Proc. Natl Acad. Sci.* **105** 18200–05
[28] Wu T and Suzuki Y 2011 *Sensors Actuators* B **156** 401–9
[29] Cao L, Hu H-H and Gao D 2007 *Langmuir* **23** 4310–4
[30] Knizikevicius R and Kopustinskas V 2004 *Vacuum* **77** 1–4
[31] Cassie A and Baxter S 1944 *Trans. Faraday Soc.* **40** 546–51
[32] Reyssat M, Yeomans J M and Quéré D 2008 *Eur. Phys. Lett.* **81** 26006
[33] Tsai P, Lammertink R G H, Wessling M and Lohse D 2010 *Phys. Rev. Lett.* **104** 116102
[34] Wilke N, Hilbert C, Brien J O' and Morrissey A 2005 *Sensors Actuators* A **123–124** 319–25
[35] Jansen H, Gardeniers H, de Boer M, Elwenspoek M and Fluitman J 1996 *J. Micromech. Microeng.* **6** 14–28